JOURNAL OF APPLIED PHYSICS **99**, 013306 (2006)

The ion cyclotron resonance frequency of short, single-species plasmas in Penning traps

S. E. Barlow[a)]
W. R. Wiley Environmental Molecular Sciences Laboratory, Pacific Northwest National Laboratory, P.O. Box 999 (K8-88), Richland, Washington 99352

Mark D. Tinkle
Dynamics Technology, Inc., 21311 Hawthorne Boulevard, Suite 300, Torrance, California 90503-5610

(Received 23 August 2005; accepted 14 November 2005; published online 12 January 2006)

We present here models that allow us to calculate the effects of various linear and low-order nonlinear terms on the $\mathbf{E}\times\mathbf{B}$ drift frequency in a cylindrical Penning trap mass spectrometer. These effects translate directly to shifts in the observed ion cyclotron resonance frequency. We show that nonlinearities in the external electrostatic potential interact with the space charge to affect the observations. Similarly, image charge effects are readily incorporated. The model is then used to describe experimental observations and found to largely account for our observations. © *2006 American Institute of Physics*. [DOI: 10.1063/1.2158504]

I. INTRODUCTION

Since the dawn of Penning trap mass spectroscopy more than 50 years ago,[1] effects due to the presence of charge have been recognized as a major factor in determining the accuracy and precision of mass determinations. The issue continues to this day, see, e.g., the excellent review by Zhang *et al.*[2] and references therein for a comprehensive discussion of the literature and methods that have been developed to deal with this problem in the analytical laboratory.

Over the last few years we have developed a set of tools that allow us to construct relatively simple models which describe the ion cloud behavior in a Penning trap.[3–6] Here we bring those tools together to develop a simple, approximate formulation of the "space-charge" problem. We find that the electric fields from the trap electrodes and trapped ion cloud are interdependent; this, in turn, makes the interpretation of observations much more difficult.

In this paper we focus on a single m/q species in a Penning trap and defer to a later publication the more challenging problems that arise when ions of different masses are studied. Not only is the single-species problem fairly simple, but anything that affects a single-ion cloud will also affect each ion bunch in a multispecies system individually. Our treatment begins with what we might call the fundamental ion cyclotron resonance (ICR) equation:

$$\omega_{\mathrm{ICR}} = \Omega - \omega_D, \tag{1}$$

where $\Omega = qB/m$ is the cyclotron frequency and ω_D is the $\mathbf{E}\times\mathbf{B}$ drift frequency. We prefer to use the term "drift" instead of either magnetron or diocotron frequency because there are important contributions from both the trap and image charge fields. To the degree that the magnetic field can be considered uniform and time independent, Eq. (1) is true. The problem thus reduces to one of finding the appropriate electric fields. The single-particle drift frequency is given by

$$\omega_D = \frac{\Omega}{2}\left(1 - \sqrt{1 - \frac{4q}{m\Omega^2}\left[\frac{E(r)}{r}\right]_{r=r_C}}\right). \tag{2}$$

Here, $E(r)$ is the radial electric field and r_C is the particle's drift or cyclotron radius. When the second term under the radical sign is sufficiently small—as will *always* be the case here—Eq. (2) simplifies to

$$\omega_D \approx \frac{1}{B}\left[\frac{E(r)}{r}\right]_{r=r_C}. \tag{3}$$

When we consider an extended charged cloud, the electric field in Eq. (3) is replaced by the electric field averaged over the cloud. This approach is a well-developed tool in high-energy beam theory, but does not seem to have been applied to the ICR.[7,8] The bulk of Sec. III is devoted to finding these average quantities. For the ion cloud system, r_C is interpreted as the "center of charge coordinate." When either drift or cyclotron motion is excited, r_C is also the magnitude of the "drift radius" $r_{C\text{-}D}$ or the "cyclotron radius" $r_{C\text{-ICR}}$.

Section II contains a brief description of our instrument that was used to obtain the data of Sec. IV. A much more detailed account can be found elsewhere.[5] In Sec. III we develop two models of the ion cloud. The first model relates the drift frequency to the trapping and ion cloud parameters and included image charge effects. The second model relates space charge to trap parameters directly. In Sec. IV these models are used to interpret data from our instrument. We show that the two very different models produce quantitatively consistent results, which gives us reassurance about the validity of the approach. Finally, we discuss some of the known weaknesses in both the model and experimental measurements—both of which can be addressed by further investigation.

Unless otherwise stated, all equations are written in *systéme International* (SI) units. With that said, the notation simplifies by using scaled distances. Thus most of the equations are written in the form $f(X,x) = g(X)h(x)$, where the

---

[a)]Author to whom correspondence should be addressed; electronic mail: se.barlow@pnl.gov

© 2006 American Institute of Physics

Downloaded 12 Feb 2007 to 128.187.0.164. Redistribution subject to AIP license or copyright, see http://jap.aip.org/jap/copyright.jsp

TABLE I. Constants for ICR from Barlow and Tinkle (Ref. 5).

Quantity	Value	Unit
Temperature T	290	K
Magnetic field (B)	7.0469	T
Trap radius (R_0)	2.000	cm
Trap length ($2Z_0$)	3.326	cm
c_2	0.934	
c_4	0	
c_6	−0.209	

capitalized quantities carry dimensions and the lower case variables are scaled. This is illustrated in Fig. 1, where the natural distance scaling is the trap radius R_0. Cylindrical coordinates (r,θ,z) or (R,θ,Z) are used throughout the paper. The origin is taken at the center of the trap electrodes with the z axis coincident with the trap's axis of cylindrical symmetry and parallel to the magnetic field. Furthermore, the charge distributions are taken as symmetric about the $z=0$ plane.

II. EXPERIMENT

The ion cyclotron resonance (ICR) mass spectrometer used for the experiments was described at length in a previous paper.[5] It consists of a cylindrical box Penning trap with an aspect ratio (length-to-diameter) of 0.8315. This aspect ratio produces an electrostatic trapping potential dominated by the harmonic $O(r^2)$ and sixth-order $O(r^6)$ anharmonic terms, see Table I. The trap is mounted in an UHV system and placed at the center of a 7 T superconducting solenoid magnet. Table I summarizes important constants associated with the trap and the data in Sec. IV. The c_n's are the coefficients of a spherical harmonic expansion of the trap's electrostatic potential.[5]

External to the bore of the magnet is a "source selector" that consists of a linear translation stage on which is mounted an electron gun, a Cs$^+$ ion gun, and an einzel lens (this last option allows ions from other sources to be introduced into the trap.[9,10]) The measurements reported here required only the use of the electron and cesium guns. The magnetic fringe field at these guns was 120 G and thus the beams are focused by a factor of 24. The initial 0.8 mm electron beam was reduced to $\sim 33\mu$ and the 5 mm Cs$^+$ beam to $\sim 210\mu$. Furthermore, if either gun was displaced horizontally or vertically from the magnet's axis, the offset at the trap was reduced by the same factor of 24.

Ions or electrons entering the trap from the source region passed through a pair of orthogonal $\mathbf{E}\times\mathbf{B}$ drift plates. We found out that they could also be used to apply a retarding potential to the beams. By adjusting the x-y position of the trap to where these plates acted symmetrically to retard the beam, the beam and trap could be brought to the center of the magnetic field $\pm 10\mu$. As described before, the trap was mounted on a gimbal that permitted angular alignment to better than 0.5 mrad (0.03°).[5] The angular and x-y adjustments were performed iteratively because the actual adjustment mechanisms were not orthogonal.

III. THE ELECTROSTATIC MODEL

Here we treat the ion cloud as a cold uniformly charged spheroid. There is considerable theoretical and experimental justifications for such a simplification.[11–15] Additional support for the model comes from accelerator physics experiments and theory, in particular, the works of Sacherer,[7] who developed the concept of "equivalent ellipsoids," and Allen and Reiser,[8] who have extended the original analysis in several important directions. For us the important result is that the gross, readily observable behaviors of the ion clouds do not generally depend on the details of the charge distribution. Rather they depend only on the first two moments of the distribution, which are the total charge and characteristic dimensions. The ellipsoid with uniform charge density has only these two moments and is therefore the simplest member of this class of distribution. We further simplify the model by assuming that the charge distributions can be described by *spheroids* whose axis of rotational symmetry is parallel to the magnetic field. This simplification greatly simplifies the math and allows certain relationships to be clearly illustrated.

A. The distribution

It is standard practice to describe spheroids in terms of eccentricities. However, the definition of eccentricity varies with the author. We choose only to define the *aspect ratio*:

$$\alpha = \frac{z_P}{r_P}. \tag{4}$$

Here, z_P is the half-length of the ion cloud and r_P is its radius; clearly, $z_P/r_P = Z_P/R_P$. The distribution function for a uniformly charged spheroid may be written as

$$n(r,z) = \frac{4}{3}\pi R_P^2 Z_P \rho \begin{cases} 1, & \dfrac{r^2}{r_P^2} + \dfrac{z^2}{z_P^2} \leq 1 \\ 0, & \dfrac{r^2}{r_P^2} + \dfrac{z^2}{z_P^2} > 1, \end{cases} \tag{5}$$

where ρ is just a constant equal to the density. The first moment of the distribution is found in the usual way,

$$N = \frac{\frac{4}{3}\pi R_P^2 Z_P}{\frac{4}{3}\pi r_P^2 z_P} \int_{-z_P}^{z_P} dz \int_0^{r_P\sqrt{1-(z/z_P)^2}} r dr \int_0^{2\pi} \rho d\theta, \tag{6}$$

where the order of integration may be changed with a suitable change of the limits of integration.

We will repeatedly need to compute averages over the volume occupied by the charge distribution, the average value of a quantity $\langle f(r,\theta,z)\rangle$ is given by

Downloaded 12 Feb 2007 to 128.187.0.164. Redistribution subject to AIP license or copyright, see http://jap.aip.org/jap/copyright.jsp

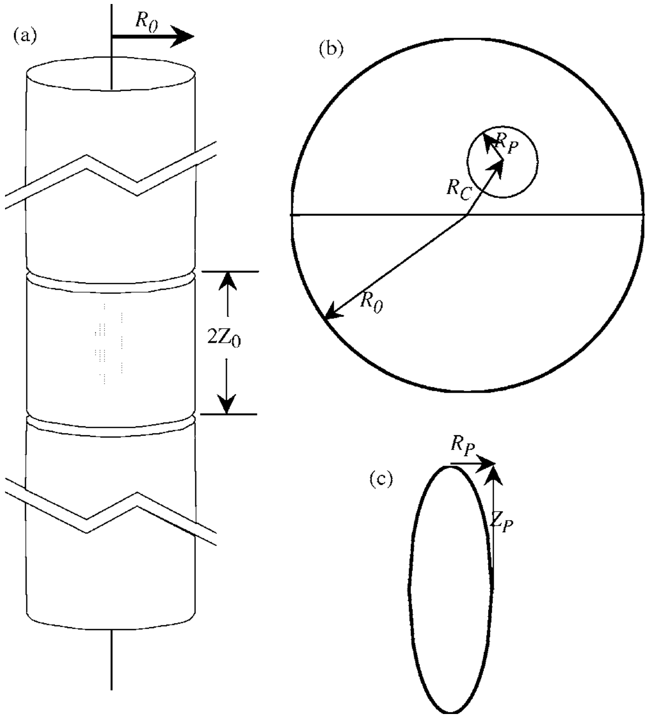

FIG. 1. (a) Cylindrical Penning trap with radius R_0 and half-length Z_0. (b) Ion cloud of radius R_P in trap. The center of the ion cloud is at R_C. The cloud rotates about its own axis at frequency $-\omega_R$ and gyrates about the trap axis with a frequency $-\omega_D$ or $-\omega_{\mathrm{ICR}}$. The z axis is directed out of the page and the charge sign is >0. (c) Sketch of spheroidal ion cloud of radius R_P and half-length Z_P.

$$\langle f(r,\theta,z)\rangle = \frac{1}{\frac{4}{3}\pi r_P^2 z_P}\int_{-z_P}^{z_P} dz \int_0^{r_P\sqrt{1-(z/z_P)^2}} r\,dr \times \int_0^{2\pi} f(r,\theta,z)\,d\theta. \tag{7}$$

During the course of a derivation, one needs to move cautiously between scaled and unscaled variables to ensure that the constant factors and dimensions are correct.

B. Trap potentials

Figure 1 and the discussion in Sec. II tacitly imply that the formalism here applies to ion clouds stored in a predominantly harmonic electrostatic well and situations where the axial extent Z_P does not exceed R_0 significantly. Thus extension to Malmberg-Penning traps[16] or the ATHENA trap[17] should proceed cautiously. For most Penning traps employed in mass spectroscopy, however, a simple spherical-harmonic expansion about the origin suffices to describe the electrostatic potentials and fields produced by the electrode structure:

$$\Phi_T(r,z) = V_T\left[c_2\left(-\frac{1}{2}r^2+z^2\right) + c_4\left(\frac{3}{8}r^4 - 3r^2z^2 + z^4\right) + c_6\left(-\frac{5}{16}r^6 + \frac{45}{8}r^4z^2 - \frac{15}{2}r^2z^4 + z^6\right) + \cdots\right], \tag{8}$$

where we have set the potential of the origin to zero. V_T is the voltage drop applied between the trapping electrodes to produce the trapping fields. The c_n's are numerical constants that depend only on the ratio Z_0/R_0, the trap's aspect ratio. The dimensions (r,z) are normalized by R_0 as described above.

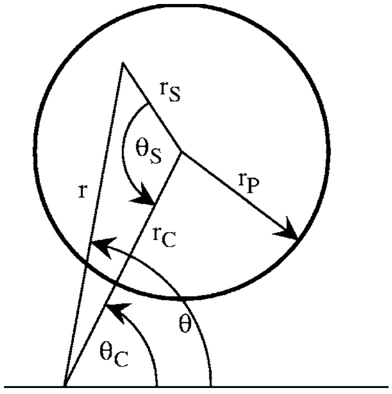

FIG. 2. Close up view of Fig. 1(b) showing the scaled and angle variables.

Referring to Fig. 2 we need to find the average radial electric field acting on a spheroid centered at $(r=r_C,\ \theta=\theta_C,\ z=0)$. This is readily accomplished by first transforming r in Eq. (8) using the law of cosines,

$$r = \sqrt{r_C^2 + r_s^2 - 2r_C r_s\cos(\theta_S)}, \tag{9}$$

then substituting into Eq. (7) and integrating. The average radial electric field is found by taking as negative the derivative of the result with respect to r_C:

$$\langle E_T(r_C)\rangle = \left(\frac{V_T}{R_0}\right) r_C\left(c_2 - \frac{3}{10}c_4[5r_C^2 - 4\{z_P^2 - r_P^2\}] + \frac{3}{56}c_6[35r_C^4 - 84r_C^2\{z_P^2 - r_P^2\} + 24\{z_P^2 - r_P^2\}^2]\right). \tag{10}$$

The form of $\langle E_T(r_C)\rangle$ can now be substituted into Eq. (2) or (3) to find the drift frequency with corrections for trap anharmonicities.

C. Image charge effects

The image charge calculation to find $\langle E_{\mathrm{im}}(r_C)\rangle$ is rather involved and only a brief outline and a few important intermediate results are given here. Somewhat surprisingly, the final form is quite simple. In a recent note Barlow[6] showed that the potential everywhere inside a long conducting cylinder due to the image charge from a point charge at $\mathbf{x}'=(r',\theta',z')$ may be written as

$$\Phi_{\mathrm{im}}(\mathbf{x}';\mathbf{x}) = \frac{q}{2\pi^2\epsilon_0 R_0}\sum_{m=0}^{\infty}\varepsilon_m\cos(m[\theta-\theta']) \times \int_0^{\infty}\frac{K_m(k)I_m(kr)I_m(kr')\cos(k[z-z'])}{I_m(k)}dk. \tag{11}$$

Here q is the charge, ϵ_0 is the permittivity of free space, ε_m equals unity when $m=0$ and 2 otherwise, and $I_m(x)$ and

Downloaded 12 Feb 2007 to 128.187.0.164. Redistribution subject to AIP license or copyright, see http://jap.aip.org/jap/copyright.jsp

$K_m(x)$ are the associated Bessel functions of the first and second kind, respectively, of order m. The fully symmetric form of Eq. (11), i.e., for $m=0$, was also given by Allen and Reiser,[8] [Eq. (27)] and can be readily derived directly from Smythe[18] (Sec. 5.351).

The first step is to find the image potential everywhere inside the cylinder due to our uniform spheroidal charge distribution centered at $(r_C, \theta_C, 0)$. This can be accomplished by moving $\cos(m[\theta-\theta'])$ inside the integral, expanding both cosine factors. Note: $\cos(x-x')=\cos(x)\cos(x')+\sin(x)\sin(x')$; the sine terms will integrate to zero eventually, and might as well be discarded at this point. Making use of this hint, we are left with a factor $I_m(kr')\cos(m\theta')$. Applying the law of cosines and an addition theorem due to Watson[19] [Eq. (11.3.7)],

$$I_m(kr')\cos(m\theta) = \sum_{n=0}^{\infty} \varepsilon_n (-1)^n I_{m+n}(kr_C) I_n(kr_s)\cos(n\theta_s), \tag{12}$$

Eq. (11) can be transformed into coordinates centered on the charge cloud. [Note: Watson placed certain requirements on the relative magnitudes of r_C and r_s in Eq. (12); however, direct computations indicated that these are unnecessary.] Substituting Eq. (12) into Eq. (11) and rearranging gives a factor $I_n(kr_s)\cos(n\theta_s)\cos(kz')$. Multiplying by ρ, this factor may be integrated over the charge distribution to get an auxiliary function $W(r_P, z_P)$:

$$aW_m(r_P,z_P) = 2\rho\int_0^{r_P} I_m(krs)rsdrs\int_0^{zp\sqrt{1-rs^2/rp^2}} \times\cos(kz')dz'\int_0^{2\pi}\cos(n\theta_s)d\theta_s, \tag{13}$$

where a is a constant to be determined. Performing the triple integral eliminates all of the sine terms mentioned above and all of the n terms except $n=0$, and we find

$$aW(r_P,z_P) = \frac{4}{3}\pi R_P^2 Z_P\rho \begin{cases} \dfrac{3\sqrt{2\pi} I_{3/2}(k\sqrt{r_P^2-z_P^2})}{2k^{3/2}(r_P^2-z_P^2)^{3/4}}, & z_P < r_P\text{:oblate} \\ 1, & z_P = r_P\text{:spherical} \\ \dfrac{3\sqrt{2\pi} J_{3/2}(k\sqrt{z_P^2-r_P^2})}{2k^{3/2}(z_P^2-r_P^2)^{3/4}}, & z_P > r_P\text{:prolate.} \end{cases} \tag{14}$$

Here $J_m(x)$ is the Bessel function of the first kind of order m and $a=(4/3)\pi R_P^2 Z_P \rho = N$, the total number of charges. The image charge potential for the spheroid is then

$$\Phi_{\text{im}}(r_C,\theta_C;r_P,z_P;r,\theta,z) = \frac{qN}{2\pi^2\epsilon_0 R_0}\sum_0^{\infty}\varepsilon_m\cos(m[\theta-\theta_C]) \times\int_0^{\infty}\frac{K_m(k)I_m(kr_C)I_m(kr)\cos(kz)}{I_m(k)}W(r_P,z_P)dk. \tag{15}$$

The average image charge forces can be found from Eqs. (7) and (15) by proceeding in the same manner as was just used to find $\Phi_{\text{im}}(r_C,\theta_C;r_P,z_P;r,\theta,z)$. The result is an "image charge pseudopotential" of the type used by Tinkle and Barlow for point charges:[4]

$$\Phi_{\text{psu}}(r_C,\theta_C;r_P,z_P) = \frac{qN}{2\pi^2\epsilon_0 R_0}\sum_0^{\infty}\varepsilon_m\cos(m\theta_C) \times\int_0^{\infty}\frac{K_m(k)I_m(kr_C)^2}{I_m(k)}W(r_P,z_P)^2 dk. \tag{16}$$

Equation (16) is rigorous but cumbersome to use. An approximate form can be found by expanding the integrand in powers of r_C and numerically integrating the result term by term. The resulting numerical solution can then be fitted as a function of $z_P^2-r_P^2$. Carrying out this procedure to r_C^4 and ignoring the constant term as unimportant here gives

$$\Phi_{\text{psu}}(r_C,0;r_P,z_P) \approx -\frac{qN}{4\pi\epsilon_0 R_0}\left(\frac{1.0027 r_C^2}{\sqrt{1+0.81[z_P^2-r_P^2]}} + \frac{1.0009 r_C^4}{[1+1.03\{z_P^2-r_P^2\}]^{7/8}}\right). \tag{17}$$

Equation (17) has a number of interesting features. First, if we set $r_P, z_P=0$ we recover the point-charge result of Tinkle and Barlow[4] as we should. Second, this result holds for very oblate through very prolate spheroids and only seems to seriously break down when $r_P\to 1$, i.e., if the spheroid nears the wall as we might suspect. Finally, the ion cloud's shape appears here in the same way as it does in the average trap fields only as $z_P^2-r_P^2$. The result in Eq. (17) applies to a long cylindrical tube, but the presence of the coefficients of Tinkle and Barlow suggests that a reasonable estimate of the effect of finite trap length can be found in their results. Thus, for the Penning trap described in Sec. II, 1.0027 would be replaced by 0.7534 and 1.0009 by 1.1243 (Ref. 4 Table II).

The average electric field on the spheroid due to its image charge in our ion trap is

$$\langle E_{\text{im}}(r_C)\rangle = -\frac{1}{2R_0}\left(\frac{\partial}{\partial r_C}\Phi_{\text{psu}}(r_C,\theta_C;r_P,z_P)\right) = \frac{qN}{8\pi\epsilon_0 R_0^2}r_C\left(\frac{2\times 0.7534}{\sqrt{1+0.81[z_P^2-r_P^2]}} + \frac{4\times 1.1243 r_C^2}{[1+1.03\{z_P^2-r_P^2\}]^{7/8}}\right). \tag{18}$$

Combining Eqs. (10) and (18) in Eq. (3) gives the drift frequency,

$$\omega_D = \frac{1}{B}\frac{V_T}{R_0}\left(c_2 - \frac{3}{10}c_4[5r_C^2 - 4\{z_P^2-r_P^2\}] + c_6[35r_C^4 - 84r_C^2\{z_P^2-r_P^2\} + 24\{z_P^2-r_P^2\}^2]\right) + \frac{1}{B}\frac{qN}{8\pi\epsilon_0 R_0^3}\left(\frac{1.5068}{\sqrt{1+0.81[z_P^2-r_P^2]}}\right.$$

Downloaded 12 Feb 2007 to 128.187.0.164. Redistribution subject to AIP license or copyright, see http://jap.aip.org/jap/copyright.jsp

$$+\frac{4.4972r_C^2}{[1+1.03\{z_P^2-r_P^2\}]^{7/8}}\Bigg). \tag{19}$$

Equation (19) relates then the trap's constants—see Table I—and the ion cloud parameters of number of charges N, diameter and length, $2r_P$, $2z_P$, and excitation amplitude r_C. The excitation amplitude can be calculated from the excitation wave form or by examining the first and third harmonics of either the drift or ICR signals, see, e.g., Barlow and Tinkle.[5] The ion cloud radius can be estimated from the electron- or ion-beam centering error by assuming that radial transport can be ignored. However, the ion number and axial extent remain unknown.

D. Space-charge model

A second relationship between the trap's parameters and those of the ion cloud is readily found. Inside the ion cloud, the axial electric field is necessarily zero, see Prasad and O'Neil.[11] That is, the trap's field is exactly cancelled by the ion cloud's space charge. Put in other words, the potential along any cylinder r inside the ion cloud is constant. From the known potential for a spheroidal charge distribution, see, e.g., Davidson (Ref. 12, p. 116), we can find the space-charge potential at $(r_s,z)=(0,z_P)$ which must cancel the trap's potential, thus

$$V_T(c_2z_P^2+c_4z_P^4+c_6z_P^6)=\frac{3q\alpha^2N}{8\pi\epsilon_0z_PR_0}\begin{cases}\dfrac{2\sqrt{1-\alpha^2}+\alpha\left[\tan^{-1}\left(\dfrac{\alpha}{\sqrt{1-\alpha^2}}\right)-\pi\right]}{2[1-\alpha^2]^{3/2}}, & \alpha<1\text{:oblate}\\[2ex] \dfrac{\alpha}{3}, & \alpha=1\text{:sphere}\\[2ex] \dfrac{2\sqrt{\alpha^2-1}-\alpha\ln[(\alpha-\sqrt{\alpha^2-1})/(\alpha+\sqrt{\alpha^2-1})]}{2[\alpha^2-1]^{3/2}}, & \alpha>1\text{:prolate},\end{cases} \tag{20}$$

where $\alpha=z_P/r_P$ as explained earlier and we have taken $r_C=0$. Generalization to $r_C>0$ is straightforward. In finding Eq. (20) we have assumed that image charge contributions can be ignored here.

Equations (19) and (20) are independent; therefore, we have two equations and two unknowns and we should be able to solve for both. Unfortunately, Eq. (20) is transcendental and not well described by any nontranscendental function, so simple relations cannot be found. The problem can be easily handled numerically, however.

IV. RESULTS

For the drift experiments, the excitation radius $R_{C\text{-}D}$ was kept small, typically $\approx 150\mu$, thereby justifying the use of Eq. (20). In the same limit, Eq. (19) simplifies to

$$\begin{aligned}\omega_D&=7.095V_T(0.934-4.94\{z_P^2-r_P^2\}^2)\\&\quad+2.554(10)^{-7}N\Bigg(\frac{1.5068}{\sqrt{1+0.81[z_P^2-r_P^2]}}\\&\quad+\frac{4.4972r_C^2}{[1+1.03\{z_P^2-r_P^2\}]^{7/8}}\Bigg),\end{aligned} \tag{21}$$

where we have substituted in universal constants and values from Table I.

A. Electron drift motion

Neither Eq. (20) nor (21) has any mass dependence, so information derived from electron drift measurements should be entirely transferable to the case of heavy positive or negative ions. According to Eq. (21) the observed drift frequency should depend on both the number of charges and shape of the ion cloud. This is illustrated in Fig. 3. Here, an electron cloud of several million electrons was produced in the trap by on-axis electron bombardment of the background gas, $V_T=30$ V, and allowed to evolve in time while monitoring the drift frequency, Figs. 3(a) and 3(b). Periodically, the drift motion was excited to check that no charge was lost, Figs.

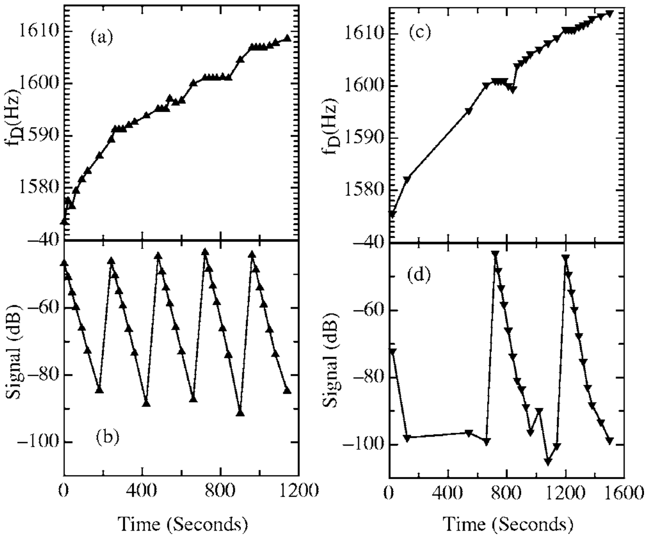

FIG. 3. (a) Time evolution of f_D for a moderate-sized electron cloud. (b) Detected amplitude of the drift signal. Note the periodic excitation indicating no loss of charge. [(c) and (d)] Measurement of (a) and (b) is repeated, but with fewer excitations and followed for longer times.

Downloaded 12 Feb 2007 to 128.187.0.164. Redistribution subject to AIP license or copyright, see http://jap.aip.org/jap/copyright.jsp

TABLE II. Electron gun offsets and electron cloud radii.

Gun offset (mm)	Beam offset (μ)	R_P (μ)
0.4	19	30
2.2	100	158
5.5	255	403

3(c) and 3(d). It is evident that the charge was stable and unaffected by the weak excitation. So the only remaining explanation of the frequency drift data is that the quantity $z_P^2 - r_P^2$ was evolving presumably due to electron-neutral collisions. These data, in a slightly different form, were presented earlier by Tinkle and Barlow (Ref. 4, Fig. 3).

In a second series of experiments, electrons were accummulated in the trap for varying lengths of time and different electron gun offsets. The electrons were allowed to relax for 5 s then the drift motion was excited. Both the amplitude of the response and drift frequency were recorded. The electron beam is assumed to produce an electron cloud whose rms radius is equal to the electron-beam offset. Table II gives the offsets and electron cloud radii.

Figure 4 shows a log-log plot of all of the response amplitude data versus fill time. Except at the shortest (<1 s) and longest (>100 s) fill time, the response versus fill time is quite linear and independent of the offset of the electron gun. Figure 5 shows the drift frequency data for these same points. The data are plotted with both linear and semilog scales to show both long-and short-fill-time behaviors. In all cases the short-fill-time drift frequency is about 1584.4 Hz. With increasing numbers of electrons the drift frequency at first increases, then levels off, and finally, drops dramatically. These features are qualitatively captured by Eq. (21). It is evident from Fig. 5 that differences in the cloud radius do translate into different frequency responses; this can be attributed to a more rapid axial growth as the electron gun was brought closer to the axis. At the longest fill times shown here, both the 30μ and 158μ frequency data start to turn around; this feature is *not* captured by our equations and is presumably due to higher-order nonlinearities becoming important.

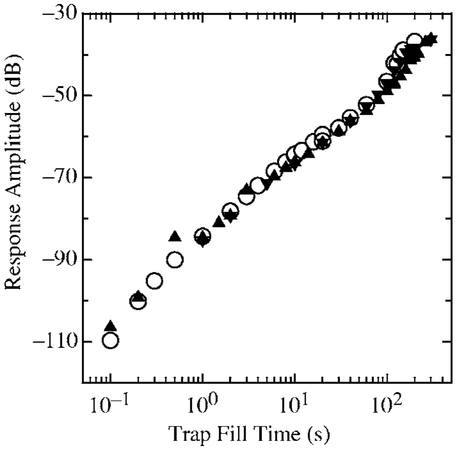

FIG. 4. Amplitude of electron drift signal vs filling time for three different radii. The response is nearly linear and independent of the filling radius. Open circles—30μ; solid triangles—158μ; inverted triangles—403μ.

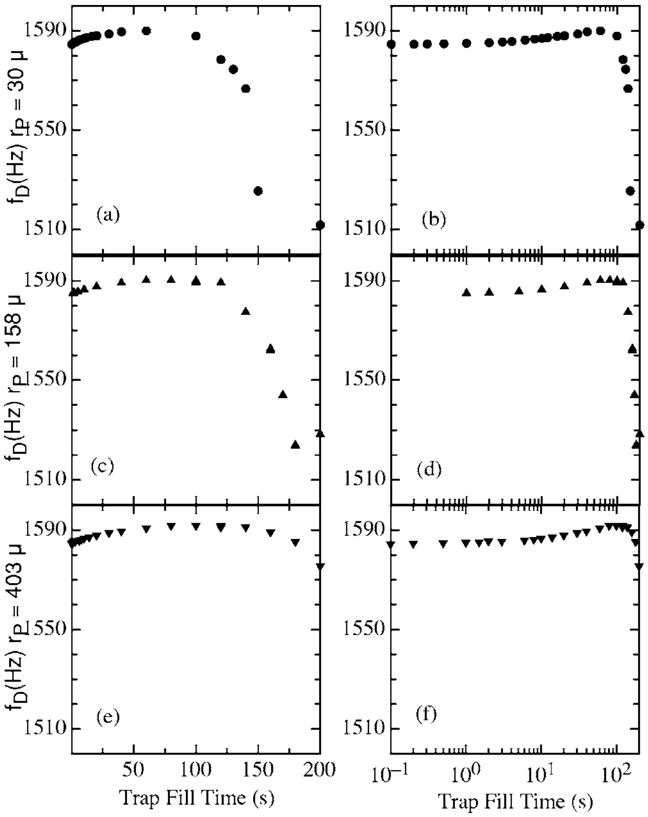

FIG. 5. Drift frequency vs filling time for the different electron cloud radii. Left-hand plots are linear in time, while right-hand plots are log time in order to illustrate both long-and short-time behaviors.

After some iterations, we find that Eqs. (20) and (21) can be solved to within our general uncertainties by taking

$$\frac{\partial}{\partial t}N = 9.8(10)^4 \text{ s}^{-1}. \tag{22}$$

Figure 6 shows plots of calculated Z_P versus fill time (a) and Z_P calculated using Eq. (21), the image charge model, and Eq. (20), the space-charge model. The close agreement between the models implies that the value for the electron number is likely correct.

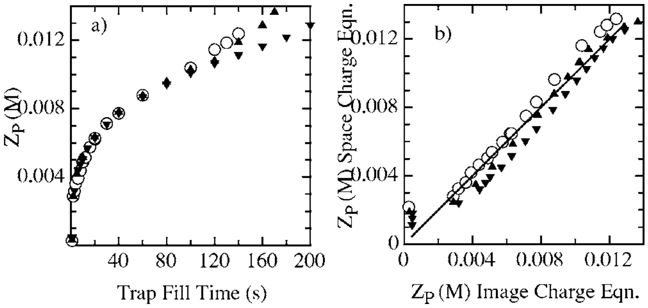

FIG. 6. Computed values of Z_P. (a) The "image charge model" was used to compute Z_P vs fill time for the different radii. (b) Comparison of the "image charge equation" with the "space-charge equation" showing that the two equations have been solved simultaneously to a good degree.

Downloaded 12 Feb 2007 to 128.187.0.164. Redistribution subject to AIP license or copyright, see http://jap.aip.org/jap/copyright.jsp

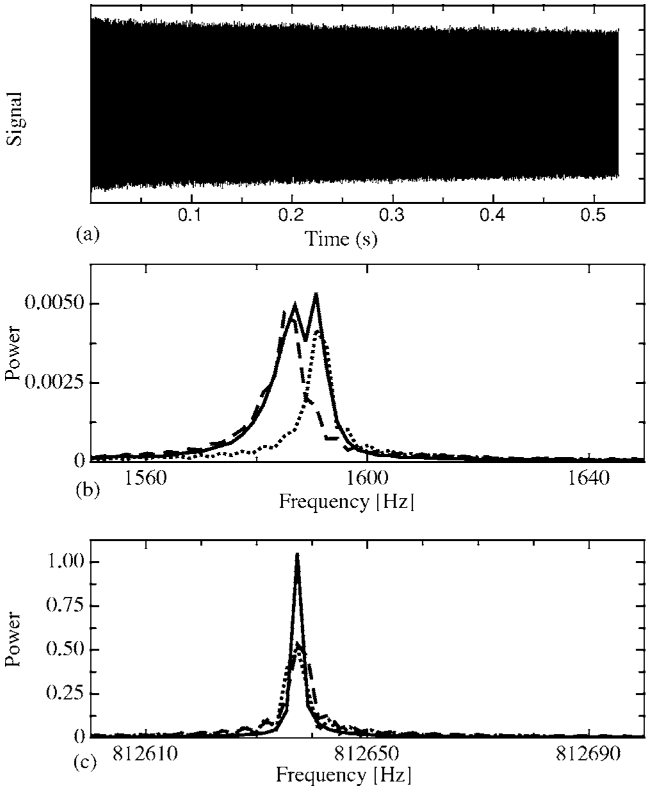

FIG. 7. Ion cyclotron resonance signal from Cs$^+$ ion cloud with a trapping potential of 30 V. (a) shows the time domain signal used to compute the power spectra in (b) and (c). In (b) and (c) the solid line is the power spectrum from the entire transient, while the dashed line comes from only the first half and the dotted line from the second half. Note that both plots (b) and (c) are 100 Hz wide.

B. Compound ICR and drift motion

Up to this point we have tacitly assumed that either drift or cyclotron motion, but not both, was excited. In the more general case, both modes are excited, as illustrated in Fig. 7. Here, a fairly large cesium ion cloud ($N > 10^6$) with $V_T = 30$ V was trapped and allowed to relax. The cloud was excited by a rapid-frequency chirp to an estimated cyclotron radius of $r_{C\text{-ICR}} = 1.5$ mm. Figure 7(a) shows the resulting time domain signal and illustrates the relatively modest damping that can readily be achieved.

Close examination of the power spectrum reveals some important details. Figure 7(b) shows the signal from the drift motion, which was excited by the rapid on and off components of the chirp pulse. Figure 7(c) shows the ICR signal, the full width at half maximum of this line is ≈ 2.5 Hz—essentially transform limited. In contrast, the drift signal is nearly 10 Hz wide and shows a distinct double peak. The dashed and dotted lines in both spectra were found from the first and second halves of the time series data, respectively. Clearly, the frequency of the actual drift motion has increased by around 5 Hz during the course of measurement. The frequency evolution is consistent with either an increase of the ion cloud's radius or a diminution of the radius of drift motion—see Eq. (19) and Figs. 3—or both. The time scales in Figs. 3 and 7 are vastly different, but this is readily understood in that the cyclotron motion, with considerable kinetic energy, couples through the nonlinear terms to the other motions and thus provides a source of free energy to drive the evolution of the ion cloud and drift motion. No quantitative treatment of this type of damping mechanism exists.

A second, more important point illustrated in Fig. 7 is that the shift of the drift frequency has no effect on the ICR frequency, in apparent violation of the discussion associated with Eq. (1). This can be resolved by noting that we have until now only considered circular orbits. The epitrochoidal motion resulting from both drift and cyclotron motions is easily resolved into cyclotron motion with a characteristic "cyclotron radius" $r_{C\text{-ICR}}$ and a drift motion with a characteristic orbital radius $r_{C\text{-}D}$. Substituting $r_{C\text{-}D}$ into Eq. (19) gives an estimate of the drift frequency, while substitution of $r_{C\text{-ICR}}$ into Eq. (19), then into Eq. (1), gives the observed ICR frequency. One as yet unanswered question is whether the quantity $z_P^2 - r_P^2$ is the same in both cases. If they are, then the frequency drift in Fig. 7 must be due primarily to a diminution of $r_{C\text{-}D}$. In any case, the use of the measured drift frequency in Eq. (1) is at best only a fair approximation in the presence of significant nonlinearities.

V. CONCLUSION

Perhaps the most surprising result is the relative simplicity of Eq. (19). It is interesting to note that the ion cloud's shape always appears in the form $z_P^2 - r_P^2$. In spite of the relative simplicity of Eq. (19), it seems plain that no *simple* mass calibration is likely to capture the behavior of the ion cloud. Many of the parametric dependences of Eq. (19) are already well known. That is, one way to reduce the variability of the electrostatic contribution to ICR mass measurements is to simply reduce ω_D in general. Increasing the magnetic field and trap size and/or reducing the trapping potential all act to reduce the magnetron frequency linearly. The nonlinear trapping terms are reduced even more rapidly with increasing trap dimension as is the image charge (diocotron) term.

At this point, the foregoing developments should be considered more suggestive than definitive. The approximations involved in the derivation merit scrutiny as do those in the analysis of the previous section. Two particular weaknesses stand out. First, in the derivation, we took the ion cloud's shape as spheroidal rather than ellipsoidal. This greatly simplified the math, but ignored the potentially important distortions due to the nonlinearities of the external field[7] and, possibly more important, the x-y quadrupole distortion of image charge. Fine[20] has shown for long columns in the Malmberg-Penning that the quadrupole distortion can come to dominate other perturbations. Second, the assumption that r_P was constant is questionable.

The model presented here does make specific, testable predictions and it would be interesting to see how well the model does—particularly in the more standard ICR traps. It would also be useful to incorporate additional diagnostic measurements. For example, Tinkle *et al.*[21] show how Dubin's theory of ion cloud modes[22] can be exploited to find the aspect ratio α. Similar methods were recently reported by the ATHENA antimatter trapping group at CERN.[17]

Downloaded 12 Feb 2007 to 128.187.0.164. Redistribution subject to AIP license or copyright, see http://jap.aip.org/jap/copyright.jsp

ACKNOWLEDGMENTS

The research described in this article was performed at the W. R. Wiley Environmental Molecular Sciences Laboratory, a national scientific user facility sponsored by the U.S. Department of Energy's Office of Biological and Environmental Research and located at the Pacific Northwest National Laboratory (PNNL). PNNL is operated by Battelle for the U.S. Department of Energy. The authors would also like to thank Dr. Julia Laskin of PNNL and Dr. Christopher Allen of LANL for useful discussions.

[1] H. Sommer, H. Thomas, and J. Hipple, Phys. Rev. **82**, 697 (1951).

[2] L.-K. Zhang, D. Rempel, B. N. Pramanik, and M. L. Gross, Mass Spectrom. Rev. **24**, 286 (2005).

[3] S. E. Barlow, A. E. Taylor, and K. Swanson, Int. J. Mass. Spectrom. **207**, 19 (2001).

[4] M. D. Tinkle and S. E. Barlow, J. Appl. Phys. **90**, 1612 (2001).

[5] S. E. Barlow and M. D. Tinkle, Rev. Sci. Instrum. **73**, 4185 (2002).

[6] S. E. Barlow, J. Appl. Phys. **94**, 6221 (2003).

[7] F. Sacherer, IEEE Trans. Nucl. Sci. **NS-18**, 1105 (1971).

[8] C. K. Allen and M. Reiser, Phys. Rev. E **55**, 7591 (1995).

[9] J. Laskin *et al.*, Anal. Chem. **74**, 3255 (2002).

[10] J. Alvarez *et al.*, Anal. Chem. **77**, 3452 (2005).

[11] S. A. Prasad and T. M. O'Neil, Phys. Fluids **22**, 278 (1979).

[12] R. C. Davidson, *Physics of Nonneutral Plasmas* (Addison-Wesley, Redwood City, CA, 1990).

[13] J. J. Bollinger *et al.*, Phys. Rev. A **48**, 525 (1993).

[14] T. M. O'Neil and D. H. E. Dubin, Phys. Plasmas **5**, 2163 (1998).

[15] D. H. E. Dubin and T. M. O'Neil, Rev. Mod. Phys. **71**, 87 (1999).

[16] J. H. Malmberg and C. F. Driscoll, Phys. Rev. Lett. **44**, 654 (1980).

[17] M. Amoretti *et al.*, Phys. Plasmas **10**, 3056 (2003).

[18] W. R. Smythe, *Static and Dynamic Electricity* (McGraw-Hill, New York, 1968).

[19] G. N. Watson, *A Treatise on the Theory of Bessel Functions*, 2nd ed. (Cambridge University Press, Cambridge, UK, 1944).

[20] K. S. Fine, Phys. Fluids B **4**, 3981 (1992).

[21] M. D. Tinkle, C. M. Surko, R. L. Spencer, and G. W. Mason, Phys. Rev. Lett. **72**, 352 (1994).

[22] D. H. E. Dubin, Phys. Rev. Lett. **66**, 2076 (1991).

Downloaded 12 Feb 2007 to 128.187.0.164. Redistribution subject to AIP license or copyright, see http://jap.aip.org/jap/copyright.jsp